

Gravity Duality of Networks

Yu Guo, Rong-Xin Miao

*School of Physics and Astronomy, Sun Yat-Sen University,
2 Daxue Road, Zhuhai 519082, China*

E-mail: guoy225@mail2.sysu.edu.cn, miaorx@mail.sysu.edu.cn

ABSTRACT: The network has been attracting increasing attention for its role in driving the artificial intelligence revolution and enabling profound insights into gravity. This paper investigates the gravity dual of the conformal field theory defined on a network (AdS/NCFT). A typical network, consisting of edges and nodes, is dual to a spacetime with branches and connecting branes, which we refer to as Net-branes. We demonstrate that the junction condition on the Net-brane results in energy conservation at the network node, providing strong support for our proposal of AdS/NCFT.

We find that the spectrum of gravitational Kaluza-Klein modes on the Net-brane is a combination of the spectra from the AdS/BCFT with Neumann boundary conditions and Dirichlet/Conformal boundary conditions, corresponding to the isolated and transparent modes, respectively. We study two-point functions for NCFTs and provide examples, such as free fields and AdS/NCFT with tensionless Net-branes. We propose that the RT surfaces intersect at the same point on the Net-brane for connected subsystems within the network and verify this with the strong additivity and monotonicity of entanglement entropy. We establish that the network entropy, defined as the difference in entanglement between NCFT and BCFT, is always non-negative and effectively illustrates the network's complexity. Finally, we briefly discuss the holographic perspective of the shortest path problem and reveal its relation to the shortest geodesic in bulk and the holographic two-point correlators of massive operators.

Contents

1	Introduction	1
2	Gravity dual of NCFT	4
2.1	Conservation law on nodes	5
2.2	Typical solutions	8
2.3	Spectrum of KK modes	10
3	Correlation functions	12
3.1	General forms	12
3.2	Free theories	14
3.2.1	Free scalar	14
3.2.2	Maxwell theory	15
3.2.3	Dirac fermions	17
3.3	Holographic theories	18
4	Holographic entanglement entropy	20
4.1	General theories	20
4.2	Network entropy	24
5	Holographic network problems	26
6	Conclusions and Discussions	28
A	Killing vectors at linear order	30

1 Introduction

Everything in the universe is interconnected, whether through interactions, quantum correlations, or entanglement. Networks offer a strong framework for studying these connections and play a crucial role in physics. Notably, neural networks are driving the recent revolution in artificial intelligence [1–3]. Additionally, tensor networks have enhanced our understanding of quantum entanglement and gravity [4–6]. Many physical systems, such as complex circuits, multi-node optical fibers, and microfluidic channels, naturally exhibit network structures. Therefore, studying physics within the context of networks is of significant theoretical and practical importance.

On the other hand, holography provides a deep insight into our understanding of gravity [7–9]. It proposes that quantum gravity in bulk is dual to a conformal field theory (CFT) on the boundary [9]. It reveals a profound connection between spacetime geometry and quantum entanglement [10]. It provides a robust framework for studying strongly

coupled systems and predicts the existence of a lower bound for fluid shear viscosity ratio entropy density [11]. Naturally, this raises the question: Can holography offer new insights into the physics of networks? For instance, what would the holographic dual of shortest-path problems be? And how might an efficient neural network manifest from a gravitational duality perspective?

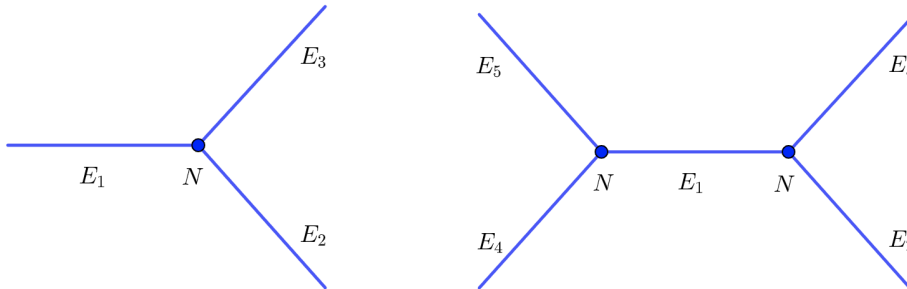


Figure 1: The networks with one node (left) and two nodes (right). The blue lines and points denote the edges (E_m) and nodes (N) of the networks.

This paper studies the CFT on networks (NCFT) and its gravity dual. A typical network includes several edges and nodes. See Fig. 1 for some examples. The nodes link the CFTs living on different edges. Thus, a key step in developing the theory of NCFT is determining the connecting conditions on the nodes. To do so, let us compare NCFT with the CFT with a boundary (BCFT). The reflective boundary condition for a BCFT reads

$$\text{BCFT} : J_n|_{\text{bdy}} = 0, \quad (1.1)$$

which means no current can flow out of the boundary. Here, n labels the normal direction, and J denotes all the currents, including the energy flux density, the electric current density, etc. For an NCFT, the current conservation suggests

$$\text{NCFT} : \sum_m J_n^{(m)}|_{\text{node}} = 0, \quad (1.2)$$

which means the total current flowing into a node is zero. Here, $J_n^{(m)}$ is the normal component of the current on the edge E_m linked by the same node. Note that since the current can flow from one edge to another, $J_n^{(m)}|_{\text{node}}$ on edge E_m can be non-zero, which is the main difference from a BCFT.

Let us go on to discuss the gravity dual. The boundary of a BCFT is dual to an end-of-the-world (EOW) brane in bulk. Takayanagi proposes to impose Neumann boundary condition (NBC) on the EOW brane [12],

$$\text{AdS/BCFT} : \left(K_{ij} - Kh_{ij} \right)|_{\text{EOW brane}} = -Th_{ij}, \quad (1.3)$$

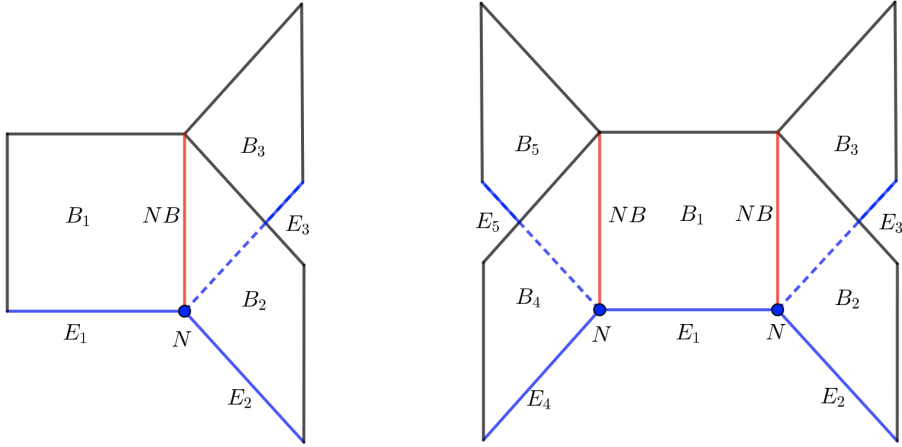


Figure 2: Geometries for holographic networks. The blue lines and points denote the edges (E_m) and nodes (N) of the networks. The red lines label the Net-branes NB , which link the branches B_m (squares) in bulk. The edges (E_m) and nodes (N) are dual to the branches B_m and Net-branes NB in bulk, respectively. For simplicity, we show only the holographic duals of the networks of Fig. 1. One can glue above geometries to get the gravity duals of arbitrary networks.

which results in (1.1) for the dual BCFTs¹. Here, K_{ij} are extrinsic curvatures, h_{ij} are induced metrics, and T is the brane tension. Similarly, the network node is dual to a brane in bulk, and we refer to it as a Net-brane. See Fig. 2 for the geometry of holographic networks. Inspired by (1.3), we propose to impose the following junction condition on the Net-brane

$$\text{AdS/NCFT} : \sum_m \left(K_{ij}^{(m)} - K h_{ij} \right) |_{\text{Net-brane}} = -T h_{ij}, \quad (1.4)$$

where $K_{ij}^{(m)}$ denote the extrinsic curvatures on bulk branches B_i . We require the induced metrics from different bulk branches into the Net-brane to be the same

$$\text{AdS/NCFT} : h_{ij} |_{\text{Net-brane}} = h_{ij}. \quad (1.5)$$

Recall that the NBC (1.3) in bulk results in the reflective boundary condition (1.1) for BCFTs. Similarly, the bulk junction condition (1.4) yields the conservation law (1.2) for NCFTs on the network node. Note that (1.4) reduces to the usual junction condition when there are only two bulk branches². It provides additional support for our proposal. It

¹It is proposed that the NBC (1.3) on the EOW brane corresponds to the reflective boundary condition (1.1) of BCFTs. We provide solid proof of this statement for AdS/BCFT and generalize it to AdS/NCFT in this paper.

²The usual junction condition on a thin shell reads $(K_{ij}^R - K^R h_{ij}) + (K_{ij}^L - K^L h_{ij}) = -T h_{ij}$, where R and L denote right and left-hand sides, and $K_{ij} = h_i^{i1} h_j^{j1} \nabla_{i1} n_{j1}$ with n_i the outpointing normal vector. Note that n_i^R and n_i^L have opposite signs in our notations.

should be mentioned that the junction condition (1.4) has recently been obtained in [13] for spacetimes with multiple boundaries, such as wormholes. Here, we have different physical motivations, focusing on the gravity dual of NCFT. In particular, our spacetime has only one boundary (the network) instead of multiple boundaries.

In this paper, we derive the junction condition (1.4) from the variational principle and prove that it leads to the conservation law (1.2) for NCFTs. We examine various geometries of AdS/NCFT and discover that the spectrum of gravitational Kaluza-Klein (KK) modes on the Net-brane is a mix of the spectra from the AdS/BCFT with NBC [12] and DBC/CBC [14, 15]. Additionally, we investigate the general forms of two-point correlation functions in NCFTs. We study examples of free theories in the CFT and the tensionless Net-brane in the gravitational dual. We show their mutual consistency and confirm that the current-current two-point functions satisfy the essential condition (1.2) at the network node. Next, we explore holographic entanglement entropy (HEE) in AdS/NCFT, which reveals interesting structures. We propose that for a connected subsystem on the network, the Ryu-Takayanagi (RT) surfaces in different bulk branches must be connected, but only on the Net-branes. Our proposal is consistent with the principles of strong additivity and monotonicity of entanglement entropy. We derive the connecting condition for RT surfaces on the Net-brane, showing it simplifies to the orthogonality condition for the RT surface and EOW brane in AdS/BCFT under Z_p symmetry. We outline several natural definitions of network entropy; one is based on the difference in entanglement entropy between NCFT and BCFT, which is always non-negative and effectively illustrates the network's structure and complexity. Finally, we briefly discuss the holographic viewpoints of famous network problems, such as the shortest path problem. We find it is closely related to the shortest geodesic in bulk and the holographic two-point correlators of massive operators.

The paper is structured as follows. In Section 2, we formulate the holographic dual of networks and demonstrate that the junction condition leads to a conservation law on the node for NCFTs. We also explore typical solutions in the AdS/NCFT framework and analyze the spectrum of gravitational KK modes on the Net-brane. Section 3 examines the general forms of two-point functions for NCFTs and provides examples, including free fields and AdS/NCFT with tensionless Net-branes. Section 4 focuses on holographic entanglement entropy. We propose that the RT surfaces intersect at the same point on the Net-brane for connected subsystems within the network and discuss potential definitions of network entropy. Section 5 addresses the holographic shortest path problem for networks, highlighting its connection to the shortest geodesic in bulk and the holographic two-point correlators of massive operators. Finally, we conclude with a discussion of open issues in Section 6. Appendix A examines the local Killing vectors in linear order.

2 Gravity dual of NCFT

This section explores the gravity dual of NCFTs. We derive the junction condition (1.4) from the variational principle in the bulk and demonstrate that it results in the conservation law (1.2) for NCFTs. We also examine typical AdS/NCFT solutions and analyze the

spectrum of KK modes on the Net-brane. For simplicity, we focus on the basic network illustrated in Fig. 1 (left). The generalization to more complex networks is straightforward.

Let us start with the geometry of the holographic networks. See Fig. 2 for examples. The simplest network comprises p edges E_m and one node N , which are dual to the branches B_m and the Net-brane NB in bulk, respectively. We have $\partial B_m = E_m \cup NB$ and $\partial(NB) = N$. The gravitational action in bulk reads

$$I = \frac{1}{16\pi G_N} \sum_m^p \int_{B_m} d^{d+1}x \sqrt{|g|} (R - 2\Lambda) + \frac{1}{8\pi G_N} \int_{NB} d^d y \sqrt{|h|} (-T + \sum_m^p K^{(m)}), \quad (2.1)$$

where $-2\Lambda = d(d-1)/l^2$ is the cosmological constant, $K^{(m)}$ is the extrinsic curvature on the Net-brane NB derived from the m -th branch B_m . We include the Gibbons-Hawking-York term $K^{(m)}$ on the Net-brane to ensure a well-defined action principle. The induced metric from different branches B_m to the Net-brane NB must remain continuous, which yields the continuity condition (1.5) $h_{ij}|_{NB} = h_{ij}$. For simplicity, we set $16\pi G_N = 1$ and $l = 1$ in the following discussions³. Taking variations of the action (2.1), we get on the Net-brane

$$\delta I|_{NB} = \int_{NB} d^d y \sqrt{|h|} \left[T h_{ij} + \sum_m \left(K_{ij}^{(m)} - K h_{ij} \right) \right] \delta h^{ij} = 0. \quad (2.2)$$

Since the induced metric on the Net-brane is dynamical, i.e., $\delta h_{ij} \neq 0$, the above equation derives the junction condition (1.4) mentioned in the Introduction.

2.1 Conservation law on nodes

Now turn to the important part of this section. Let us prove that the junction condition (1.4) yields the current conservation law (1.2) on the network node. We start with the Codazzi's equation

$$D^i (K_{ij} - K h_{ij}) = \frac{1}{2} R_{nj} = \frac{1}{4} T_{nj}^{\text{matter}}, \quad (2.3)$$

where D_i is the covariant derivative on the boundary, R_{nj} and T_{nj}^{matter} are the Ricci tensor and matter stress tensor in bulk, n and j denote the normal and tangential directions, respectively. On the AdS boundary, T_{nj}^{matter} vanishes so that no matter can flow out of the boundary. On the other hand, we have $\sum_m T_{\text{matter } nj}^{(m)} = 0$ for the conservation of energy flow on the Net-brane. As a result, (2.3) vanishes and $T_{ij} = K_{ij} - K h_{ij}$ are conserved energy-momentum tensors on both the AdS boundary E_m and the Net-brane NB (in sum sense)

$$D^i (K_{ij} - K h_{ij})|_{E_m} = 0, \quad (2.4)$$

$$\sum_m D^i (K_{ij}^{(m)} - K h_{ij})|_{NB} = 0. \quad (2.5)$$

³In general, the Newton's constant G_N and the AdS radius l can take different values on different branches B_m . We focus on the simplest case with the same G_N and l on all the branches in this paper.

By adding the Hayward term [16], we can smooth the above equations on the intersection of E_m and NB , i.e., $N = E_m \cap NB$.

Recall that at the interface, we can derive $D_{2n} = D_{1n}$ from Maxwell's equation $\nabla \cdot \mathbf{D} = 0$. We also expect the normal components of the conserved energy-momentum tensors to remain continuous across the interface. For our specific case at a node, we have the equation

$$\sum_m (K_E{}_{an} - K_E h_{an})|_N = \sum_m (K_{NB}{}_{na} - K_{NB} h_{na})|_N = -Th_{na}|_N = 0, \quad (2.6)$$

which leads to the conservation law (1.2) at node N . In this equation, n and a denote the normal and tangential directions. The terms K_K and K_{NB} represent the extrinsic curvatures on the network edges and Net-brane, respectively. We used the junction condition from equation (1.4) to derive the second equality, and $h_{an} = 0$ to achieve the final equality. This encapsulates the main physical idea behind the proof. However, two challenges remain. We need to express $K_E{}_{an} - K_E h_{an}$ in terms of the CFT stress tensor. Although these are related, they are generally different from one another. Second, there are no exact Killing vectors ξ_i , meaning we lack an exact conserved current $J^i = (K^{ij} - Kh^{ij})\xi_j$ in general spacetimes. Thus, the key equation (2.6) cannot hold exactly.

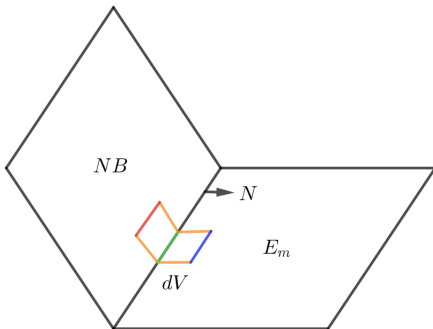


Figure 3: An infinitesimal region $dV = dldS$ covering small pieces of the Net-brane NB , the node N and network edges E_m . For simplicity, we show only one edge in the figure. The green and orange lines denote dS and dl , respectively. In all the discussions, we first take the limit $dl \rightarrow 0$ and then $dS \rightarrow 0$. The red and blue lines are labeled by S_{NB} and S_{E_m} , respectively. We have $S_{NB} = S_{E_m} = dS$ in the limit $dl \rightarrow 0$.

Now, we provide a rigorous proof that overcomes the above two difficulties. Let us choose an infinitesimal region $dV = dldS$ that encompasses small portions of the Net-brane NB , the node N , and network edges E_m . See Fig. 3, where we denote dl perpendicular to the node N and dS as the area of a small piece of N . We first take $dl \rightarrow 0$ and then $dS \rightarrow 0$ in the discussions below. In this region, spacetime is approximately flat, allowing us to select a set of local Killing vectors ξ_i that are tangential to N and obey $D_{(i}\xi_{j)} \sim O(y)$. This is done in Gauss normal coordinates $y^i = (l, y^a)$ where $dS = d^{d-1}y^a$. See Appendix A for the details of ξ_i . Starting from this setup, we derive an approximate conserved current

given by $J^i = T^{ij}\xi_j$. Integrating over the infinitesimal region gives us

$$\int_{dV} dV \sqrt{|h|} D_i \left((K^{ij} - Kh^{ij}) \xi_j \right) = \int_{dV} dV \sqrt{|h|} (K^{ij} - Kh^{ij}) D_{(i} \xi_{j)} \sim O(y) dV \rightarrow 0, \quad (2.7)$$

where we've utilized the fact that $D_{(i} \xi_{j)} \sim O(y)$ and neglected higher-order terms $O(y) dV = O(y) d^d y = O(y^{d+1})$. Applying Gauss's law leads us to

$$\sum_m \int_{S_{E_m}} dS \sqrt{|\sigma|} n^i \xi^j (K_{ij} - Kh_{ij}) = - \sum_m \int_{S_{NB}} dS \sqrt{|\sigma|} n^i \xi^j (K_{ij}^{(m)} - K h_{ij}^{(m)}), \quad (2.8)$$

where we have ignored the lateral surface areas (orange line of Fig. 3) in the limit $dl \rightarrow 0$. Here, S_{NB} and S_{E_m} are the boundaries on the Net-brane NB , and network edges E_m , which correspond to the red and blue lines in Fig. 3. By applying the junction condition (1.4) together with $n^i \xi^j h_{ij} = O(y^2) \rightarrow 0$, we find the right-hand-side of (2.8) vanishing and derive

$$\sum_m \int_{S_{E_m}} dS \sqrt{|\sigma|} n^i \xi^j K_{ij} = O(y^2) dS \rightarrow 0. \quad (2.9)$$

As shown in Fig. 3, S_{E_m} approaches the piece dS of the node in the limit $dl \rightarrow 0$. For arbitrary local Killing vectors $\xi^j \sim O(1)$ on the node and small dS , the above equation simplifies to

$$\sum_m \int_{S_{E_m}} dS \sqrt{|\sigma|} n^i K_{il} P^l_j |_{S_{E_m}} = O(y^2) \rightarrow 0, \quad (2.10)$$

where $P_{ij} = h_{ij} - n_i n_j$ is the induced metric on the node N . Note that the above derivations hold under the assumptions of Gauss normal coordinates.

In the Fefferman-Graham (FG) gauge, the induced metric on the edges E_m (the AdS boundary at $z = \epsilon$) is given by

$$ds^2 = \frac{(\eta_{ij} + \frac{\epsilon^d}{d} T_{ij}^{\text{CFT}} + \dots) dx^i dx^j}{\epsilon^2}, \quad (2.11)$$

where $x^i = (x, x^a)$ with the node at $x = 0$, T_{ij}^{CFT} represents the stress tensors of CFTs and ... denotes higher-order terms in ϵ . For the metric given above, we find that $\sqrt{|\sigma|} \sim \frac{1}{\epsilon^{d-1}}$, $n^i \sim -\epsilon \delta_x^i$, and the extrinsic curvatures (from the bulk to the network edges) are

$$\hat{K}_{ij} \sim \frac{\eta_{ij} - \frac{(d-2)}{2d} \epsilon^d T_{ij}^{\text{CFT}}}{\epsilon^2}. \quad (2.12)$$

It is important to note that $x^i = (x, x^a)$ are not the Gauss normal coordinates for non-zero T_{xi}^{CFT} . Transforming to the Gauss normal coordinates $y^i = (l, y^a)$, we have

$$dl = \left(1 + \frac{\epsilon^d}{2d} T_{xx}^{\text{CFT}}\right) dx + \frac{\epsilon^d}{d} T_{xa}^{\text{CFT}} dx^a + O(\epsilon^{d+1}), \quad dy^a = dx^a + O(\epsilon^d). \quad (2.13)$$

Note that this Gauss normal coordinates differs from the one in the Appendix A by a constant Weyl factor $\frac{1}{\epsilon^2}$. From this, we can derive the normal-tangential components of the extrinsic curvatures

$$K_{la} = \frac{\partial x^i}{\partial l} \frac{\partial x^j}{\partial y^a} \hat{K}_{ij} \sim -\frac{\epsilon^{d-2}}{2} T_{xa}^{\text{CFT}}. \quad (2.14)$$

Substituting the expression for K_{la} along with $\sqrt{|\sigma|} \sim \frac{1}{\epsilon^{d-1}}$, $n^i \sim -\epsilon \delta_l^i$ into (2.10), and taking $S_{E_m} \rightarrow dS$ on N , we subsequently demonstrate that the junction condition on the Net-brane leads to the energy conservation law on the network node

$$\sum_m \left(T_{na}^{\text{CFT}} \right)_N = 0. \quad (2.15)$$

The following subsection will verify this conservation law in the perturbative Poincaré AdS.

Under the Z_p symmetry, AdS/NCFT with p edges linked by one node simplifies to AdS/BCFT with an EOW brane. Correspondingly, the junction condition (1.4) on the Net-brane reduces to NBC (1.3) on the EOW brane. Thus, the above discussions confirm that the AdS/BCFT with NBC (1.3) is dual to the BCFT with a reflective boundary condition (1.1). On the other hand, since the Dirichlet boundary condition (DBC) fixed the induced metric rather than the extrinsic curvatures on the EOW brane, i.e., $K_{ij} - K h_{ij} \neq -T h_{ij}$, the key equation (2.6) in the proof no longer holds. Consequently, the AdS/BCFT with DBC [14] corresponds to the BCFT in an open system with a transparent boundary condition $J_n|_{\text{bdy}} \neq 0$ ⁴. We will explore this interpretation and its relevance to open quantum systems in future articles. In section 2.3, we will show that AdS/BCFT with DBC contributes to the transparent modes of AdS/NCFT.

2.2 Typical solutions

This subsection studies some typical solutions for the holographic networks, starting with the simplest example with p edges E_m linked by one node N . The bulk metric in branch B_m is given by

$$\text{Poincaré AdS} : ds^2 = \frac{dz^2 - dt^2 + dx^2 + \delta_{ab} dy^a dy^b}{z^2}, \quad (2.16)$$

where the network edge is at $z = 0$, the node is at $z = x = 0$ and the Net-brane is located at

$$\text{Net-brane} : x = -\sinh(\rho)z. \quad (2.17)$$

Then the junction condition (1.4) on the Net-brane determines the brane tension

$$T = p(d-1) \tanh \rho. \quad (2.18)$$

This Poincaré AdS is dual to the vacuum state of NCFTs on the simplest network.

⁴We remark that the AdS/BCFT with DBC fixes the tangential instead of the normal components of currents on the boundary. We will discuss this problem in details in other papers.

Let's discuss general networks that consist of at least two nodes or one loop. The Poincaré AdS (2.16) is still a gravity dual for these networks, but does not represent the vacuum state ⁵. That is because Poincaré AdS has a holographic stress tensor of zero, $\langle T_{ij} \rangle = 0$, which cannot correspond to the vacuum of networks that have a non-trivial Casimir effect (where $\langle T_{ij} \rangle \neq 0$). To illustrate this, imagine a wave traveling along an edge between two nodes. When the wave reaches a node, some is transmitted while some is reflected. It makes the node act like a partially transparent boundary, and the edge behaves like a thin, transparent strip. Consequently, the Casimir effect here is weaker than that of a solid strip, yet it is still non-zero. This reasoning also applies to the network with loops. Please refer to [19] for discussing the Casimir effect on networks. We expect that the gravity dual for the vacuum of general networks will involve the glue of Poincaré AdS for the external edges and AdS solitons for the internal edges. However, we will leave these discussions for future work and concentrate on simpler solutions in this paper.

Let us go on to discuss the gravity duals of thermal states of NCFTs. There are two typical solutions. The first one is the black string. For the simplest networks, the bulk metric in each branch reads

$$\text{Black string : } ds^2 = dr^2 + \cosh^2 r \frac{\frac{dw^2}{h(w)} - h(w)dt^2 + \delta_{ab}dy^a dy^b}{w^2}, \quad (2.19)$$

where $h(w) = 1 - w^{d-1}/w_h^{d-1}$, the network edge is located at $r = -\infty$, the node is at $r = -\infty, w = 0$, and the Net-brane with brane tension (2.18) is at

$$\text{Net-brane : } r = \rho. \quad (2.20)$$

The second one is the black hole

$$\text{Black hole : } ds^2 = \frac{\frac{dz^2}{f(z)} - f(z)dt^2 + dx^2 + \delta_{ab}dy^a dy^b}{z^2}, \quad (2.21)$$

where $f(z) = 1 - z^d/z_h^d$, the network edge is located at $z = 0$, the node is at $z = x = 0$, and the Net-brane is at

$$\text{Net-brane : } x = 0. \quad (2.22)$$

For the AdS black hole (2.21), the junction condition (1.4) is obeyed only if the brane tension is zero, $T = 0$. It is the main drawback compared to the black string (2.19). The advantage is that, like the Poincaré AdS, we can glue the AdS black hole solutions (2.21) to get the gravity duals for the general networks. See the example in Fig. 2 (right).

To end this section, we will examine the perturbations of the AdS Poincaré metric and confirm that the junction condition (1.4) in bulk leads to the energy conservation law (1.2) at the node. For our analysis, we take the following ansatz for a perturbative metric

$$ds^2 = \frac{dz^2 - dt^2 + dx^2 + \frac{2}{d}f_m(z, x)dtdx + \delta_{ab}dy^a dy^b}{z^2}, \quad (2.23)$$

⁵One should choose the brane tensions carefully to avoid the intersections of Net-branes. We focus on non-singular Net-branes in this paper.

where $f_m(z, x)$ represents the linear perturbation in the branch B_m . By solving Einstein's equations in linear order, we get

$$f_m(z, x) = X_m(x) + c_m z^d, \quad (2.24)$$

where $X_m(x)$ is an arbitrary function. The junction condition (1.4) on the Net-brane (2.17) yields one independent equation

$$\cosh(\rho) \sum_m c_m = 0. \quad (2.25)$$

The continuity condition (1.5) gives us

$$\sinh(\rho) \left(c_m z^d + X_m(-z \sinh \rho) \right) = c(z) \quad (2.26)$$

with $c(z)$ a function independent of c_m . This continuity condition is satisfied automatically in the tensionless case $\rho = 0$. In the tensile case $\rho \neq 0$, we solve $X_m(x) = b(x) - c_m x^d / (-\sinh(\rho))^d$ with $b(x)$ a general function of x , which is identical in every branch. From (2.11, 2.23, 2.24), we derive the holographic stress tensor for NCFT

$$T_{xt}^{(m)\text{CFT}} = c_m. \quad (2.27)$$

Then the junction condition (2.25) yields the conservation law for energy flux at the node

$$\sum_m T_{xt}^{(m)\text{CFT}}|_N = \sum_m c_m = 0. \quad (2.28)$$

2.3 Spectrum of KK modes

This subsection studies the gravitational KK modes on the Net-brane. We focus on the simplest network with p edges linked by one node for simplicity. In each bulk branch B_m , we take the following ansatz of the perturbative metric

$$ds^2 = dr^2 + \cosh^2(r) \left(\bar{h}_{ij}^{(0)}(y) + \epsilon \bar{H}(r) \bar{h}_{ij}^{(1)}(y) \right) dy^i dy^j + O(\epsilon^2), \quad (2.29)$$

where $\bar{h}_{ij}^{(0)}$ is the AdS metric with a unit radius and $\bar{h}_{ij}^{(1)}$ denotes the perturbation obeying the transverse traceless gauge

$$\bar{D}^i \bar{h}_{ij}^{(1)} = 0, \quad \bar{h}^{(0)ij} \bar{h}_{ij}^{(1)} = 0, \quad (2.30)$$

where \bar{D}_i is the covariant derivative with respect to $\bar{h}_{ij}^{(0)}$. Separating variables of the linearized Einstein equations, we obtain

$$(\bar{\square} + 2 - M^2) \bar{h}_{ij}^{(1)}(y) = 0, \quad (2.31)$$

$$\cosh^2(r) \bar{H}''(r) + d \sinh(r) \cosh(r) \bar{H}'(r) + M^2 \bar{H}(r) = 0, \quad (2.32)$$

where M denotes the mass of gravitons on the Net-brane. Solving (2.32) and imposing Dirichlet boundary condition (DBC) on the AdS boundary $\overset{(m)}{H}(-\infty) = 0$, we get

$$\overset{(m)}{H}(r) = \overset{(m)}{c} H(r) = \overset{(m)}{c} \begin{cases} \operatorname{sech}^{\frac{d}{2}}(r) P_{l_M}^{\frac{d}{2}}(-\tanh r), & \text{even } d, \\ \operatorname{sech}^{\frac{d}{2}}(r) Q_{l_M}^{\frac{d}{2}}(-\tanh r), & \text{odd } d. \end{cases} \quad (2.33)$$

where $\overset{(m)}{c}$ are constants, P and Q denote the Legendre polynomials, and l_M is given by

$$l_M = \frac{1}{2} \left(\sqrt{(d-1)^2 + 4M^2} - 1 \right). \quad (2.34)$$

We assume the location of the Net-brane remains invariant under linear perturbation

$$\text{Net-brane : } r = \rho + O(\epsilon^2). \quad (2.35)$$

Applying the junction condition (1.4) and the continuity condition (1.5) on the Net-brane, we obtain

$$\sum_{m=1}^p \overset{(m)}{H}'(\rho) = 0 \rightarrow \sum_{m=1}^p \overset{(m)}{c} H'(\rho) = 0, \quad (2.36)$$

$$\overset{(i)}{H}(\rho) = \overset{(j)}{H}(\rho) \rightarrow \overset{(i)}{c} H(\rho) = \overset{(j)}{c} H(\rho). \quad (2.37)$$

Solving these boundary conditions gives us one class of modes that satisfy Neumann boundary conditions (NBC)

$$\text{NBC : } H'(\rho) = 0, \quad \overset{(i)}{c} = \overset{(j)}{c}, \quad (2.38)$$

and $(p-1)$ classes of modes that satisfy Dirichlet boundary conditions (DBC)

$$\text{DBC : } H(\rho) = 0, \quad \sum_{m=1}^p \overset{(m)}{c} = 0. \quad (2.39)$$

Interestingly, the spectrum of AdS/NCFT combines characteristics from both AdS/BCFT with NBC [12] and DBC/CBC [14, 15]. Here, CBC refers to the conformal boundary condition, which yields a spectrum identical to that of DBC [15]. For discussions on the spectra of AdS/BCFT with various boundary conditions, please refer to [15]; we will not repeat those details here. It is important to note that the spectrum is positive, satisfying $M^2 > 0$, and there exists an approximate massless mode with $M^2 \rightarrow 0$ in the large tension limit as $\rho \rightarrow \infty$.

As discussed in section 2.1, the AdS/BCFT with NBC corresponds to the BCFT with a reflective boundary condition $J_n|_N = 0$. It indicates that the modes are confined to one edge and cannot flow to the other edges, which we refer to as isolated modes. On the other hand, the AdS/BCFT with DBC/CBC corresponds to an open system characterized by the transparent boundary condition $J_n|_N \neq 0$. In this case, the modes can flow freely between different edges; we call these modes transparent modes.

To summarize, we have derived the junction condition (1.4) on the Net-brane and proved that it leads to the conservation law (1.2) on the network node. We discuss several typical solutions to AdS/NCFT and verify the node conservation law (1.2) in the perturbative AdS. We find that the spectrum of gravitational KK modes on the Net-brane combines those of AdS/BCFT with NBC and DBC/CBC, which correspond to the isolated and transparent modes, respectively.

3 Correlation functions

In this section, we study the two-point functions of scalar operators and stress tensors for the NCFTs on the simplest network with p edges linked by one node. We first discuss the general constraint on two-point correlators from conformal symmetries and conservation laws. Then, we study examples of free theories and the AdS/NCFT with tensionless Net-branes. Interestingly, these two special theories have the similar structures of two-point functions.

3.1 General forms

Let us start with the symmetric group of NCFT in a flat d -dimensional Euclidean space. We denote the coordinates of the network as $\binom{(m)}{x}^\mu = (\binom{(m)}{x}, \binom{(m)}{y}^a)$, where $m = 1, \dots, p$ indicates different edges and $a = 2, \dots, d$ represents the transverse directions. The node is situated at $\binom{(m)}{x} = 0$. Similar to BCFTs [20], the symmetry group of NCFTs that keeps the node location $\binom{(m)}{x} = 0$ unchanged is reduced from the full conformal group $O(d+1, 1)$ to $O(d, 1)$. The transformations for the $(d-1)$ -dimensional translations, $O(d-1)$ rotations, and scale changes are given by

$$\binom{(m)}{y}^a \rightarrow \binom{(m)}{y}^a + \xi^a, \quad \binom{(m)}{y}^a \rightarrow R_b^a \binom{(m)}{y}^b, \quad \binom{(m)}{x}^\mu \rightarrow \lambda \binom{(m)}{x}^\mu. \quad (3.1)$$

To maintain the distance $|\binom{(m)}{x} - \binom{(n)}{x}|$ (up to a scale factor) between points on different edges, the transformations ξ^a , R_b^a , and λ must take the same values in all edges. The special conformal transformations leaving $\binom{(m)}{x} = 0$ invariant read

$$\binom{(m)}{x}^\mu \rightarrow \frac{\binom{(m)}{x}^\mu + b^\mu \binom{(m)}{x}^2}{\Omega(\binom{(m)}{x})}, \quad \Omega(x) = 1 + 2b \cdot x + b^2 x^2, \quad (3.2)$$

where $b^\mu = (0, b^a)$. For the same reason, b^μ takes the same values in all the edges.

It is straightforward to construct two invariants under the above conformal transformations

$$v_I^2 = \frac{(\binom{(m)}{y}_a - \binom{(m)'}{y}_a)^2 + (\binom{(m)}{x} - \binom{(m)'}{x})^2}{(\binom{(m)}{y}_a - \binom{(m)'}{y}_a)^2 + (\binom{(m)}{x} + \binom{(m)'}{x})^2}, \quad (3.3)$$

$$v_{II}^2 = \frac{(\binom{(m)}{y}_a - \binom{(n)'}{y}_a)^2 + (\binom{(m)}{x} + \binom{(n)'}{x})^2}{(\binom{(m)}{y}_a - \binom{(n)'}{y}_a)^2 + (\binom{(m)}{x} - \binom{(n)'}{x})^2}, \quad (3.4)$$

where v_I^2 and v_{II}^2 are invariants on the same and mixed edges, respectively. Note that, since $\binom{(m)}{x} \geq 0$, we have $|\binom{(m)}{x} - \binom{(m)}{x'}|^2 = (\binom{(m)}{y_a} - \binom{(m)}{y'_a})^2 + (\binom{(m)}{x} - \binom{(m)}{x'})^2$, while $|\binom{(m)}{x} - \binom{(n)}{x'}|^2 = (\binom{(m)}{y_a} - \binom{(n)}{y'_a})^2 + (\binom{(m)}{x} + \binom{(n)}{x'})^2$ in our notations. The two point functions of scalar operators take the following form

$$\langle O(x)O(x') \rangle = \begin{cases} \frac{F_I(v_I)}{|\binom{(m)}{x} - \binom{(m)}{x'}|^{2\Delta}}, & \text{same edge,} \\ \frac{F_{II}(v_{II})}{|\binom{(m)}{x} - \binom{(n)}{x'}|^{2\Delta}}, & \text{mixed edge,} \end{cases} \quad (3.5)$$

where Δ denotes the conformal dimension. In general, $F_I(v)$ and $F_{II}(v)$ are two independent functions. Due to the similar restricted conformal group $O(d, 1)$, the two-point correlators take similar forms for NCFTs and BCFTs. The main difference is that NCFTs have more independent functions than BCFTs in the correlation functions.

Let us go on to discuss the two-point functions of stress tensors. The restricted conformal group $O(d, 1)$ determines on the same edge [20, 21]

$$\begin{aligned} \langle T_{ij}(\mathbf{x})T_{kl}(\mathbf{x}') \rangle &= \frac{1}{s^{2d}} [\delta(v)\delta_{ij}\delta_{kl} + \epsilon(v)(I_{ik}I_{jl} + I_{il}I_{jk}) + (\beta(v) - \delta(v))(\hat{X}_i\hat{X}_j\delta_{kl} + \hat{X}'_k\hat{X}'_l\delta_{ij}) \\ &\quad - (\gamma(v) + \epsilon(v))(\hat{X}_i\hat{X}'_kI_{jl} + \hat{X}_j\hat{X}'_lI_{ik} + \hat{X}_i\hat{X}'_lI_{jk} + \hat{X}_j\hat{X}'_kI_{il}) \\ &\quad + (\alpha(v) - 2\beta(v) + 4\gamma(v) + \delta(v) + 2\epsilon(v))\hat{X}_i\hat{X}_j\hat{X}'_k\hat{X}'_l], \end{aligned} \quad (3.6)$$

where

$$\begin{aligned} v &= \frac{s}{\bar{s}} = \sqrt{\frac{(x-x')^2 + (y_a - y'_a)^2}{(x+x')^2 + (y_a - y'_a)^2}}, \\ I_{ij} &= \delta_{ij} - 2\frac{(x_i - x'_i)(x_j - x'_j)}{s^2}, \\ \hat{X}_i &= \frac{1}{s\bar{s}}(x^2 - x'^2 - (y_a - y'_a)^2, 2x(y_a - y'_a)), \\ \hat{X}'_i &= \frac{1}{s\bar{s}}(x'^2 - x^2 - (y_a - y'_a)^2, -2x'(y_a - y'_a)). \end{aligned} \quad (3.7)$$

For simplicity, we have ignored $\binom{(m)}$ for coordinates and I for all functions on the same edge. On the mixed edges, the two-point functions of stress tensors still take the form (3.6), with v replaced by v_{II} defined in (3.4), and $x' = (x', y'_a)$ of I_{ij} , \hat{X}_i , \hat{X}'_i replaced with $\bar{x}' = (-x', y'_a)$. To be consistent with the conservation law (1.2), we require

$$\sum_m \lim_{\binom{(m)}{x} \rightarrow 0} \langle T_{na}(\mathbf{x})T_{kl}(\mathbf{x}') \rangle = 0, \quad (3.8)$$

which yields the constraints

$$\gamma(v_I = 1) - (p-1)\gamma(v_{II} = 1) = 0, \quad (3.9)$$

where p denotes the number of edges.

In the following subsections, we will calculate the two-point functions of stress tensors for free NCFTs and AdS/NCFT with tensionless Net-branes. We verify that they all obeys the constraints (3.9).

3.2 Free theories

This subsection studies the two-point functions of stress tensors for free theories, including scalars, vectors and fermions.

3.2.1 Free scalar

We start with the Euclidean action for a conformally coupled free scalar

$$I = \frac{1}{2} \sum_{m=1}^p \int_{E_m} d^d x \delta^{ij} \partial_i^{(m)} \phi \partial_j^{(m)} \phi, \quad (3.10)$$

where we have ignored the curvature term in flat space. Taking variations of the action, we get the following boundary term on the node

$$\delta I|_N = \sum_m \int_N d^{d-1} y \partial_n^{(m)} \phi \delta \phi = 0, \quad (3.11)$$

which yields the junction condition (JC) for scalars

$$\text{scalar JC: } \sum_{m=1}^p \partial_n^{(m)} \phi|_N = 0, \quad \phi|_N = \phi|_N. \quad (3.12)$$

The above JC is consistent with the conservation of energy flow on the node [19]

$$\sum_{m=1}^p T_{na}^{(m)}|_N = 0, \quad (3.13)$$

where n, a denote the normal and tangential directions, and the stress tensors read

$$\begin{aligned} T_{ij} &= \partial_i \phi \partial_j \phi - \frac{1}{4} \frac{1}{d-1} ((d-2) \partial_i \partial_j + \delta_{ij} \partial^2) \phi^2 \\ &= \frac{1}{2(d-1)} (d \partial_i \phi \partial_j \phi - (d-2) \phi \partial_i \partial_j \phi - \delta_{ij} (\partial \phi)^2) \end{aligned} \quad (3.14)$$

We solve the two-point function of scalars obeying the above JC as

$$\langle \phi(x) \phi(x') \rangle = \frac{\kappa}{d-2} \cdot \begin{cases} \frac{1+c_r v_I^{d-2}}{|x^{(m)} - x'^{(m)}|^{d-2}}, & \text{same edge,} \\ \frac{c_t}{|x^{(m)} - x'^{(n)}|^{d-2}}, & \text{mixed edge,} \end{cases} \quad (3.15)$$

where

$$\kappa = \frac{\Gamma(\frac{d}{2})}{2\pi^{d/2}}, \quad c_r = -\frac{p-2}{p}, \quad c_t = \frac{2}{p}. \quad (3.16)$$

From (3.15,3.14), we derive the two-point function of stress tensors (3.6) with

$$\alpha(v_I) = \kappa^2 \left(1 + c_r^2 v_I^{2d} + \frac{c_r}{4} (d-2) d \frac{d+1}{d-1} v_I^{d-2} (1 - v_I^2)^2 \right), \quad (3.17)$$

$$\gamma(v_I) = -\frac{\kappa^2 d}{2(d-1)} \left(1 - c_r^2 v_I^{2d} + \frac{c_r}{2} (d-2) \frac{d+1}{d-1} v_I^{d-2} (1 - v_I^4) \right), \quad (3.18)$$

$$\epsilon(v_I) = \frac{\kappa^2 d}{2(d-1)} \left(1 + c_r^2 v_I^{2d} \right) + \frac{c_r}{4} \frac{\kappa^2 d}{(d-1)^2} \left((d-2)(v_I^{d-2} + v_I^{d+2}) + 2d v_I^d \right), \quad (3.19)$$

for the same edge and

$$\alpha(v_{II}) = c_t^2 \kappa^2, \quad \gamma(v_{II}) = -\frac{c_t^2 \kappa^2 d}{2(d-1)}, \quad \epsilon(v_{II}) = \frac{c_t^2 \kappa^2 d}{2(d-1)}, \quad (3.20)$$

for the mixed edge. Other functions of (3.6) can be derived with tracelessness of stress tensor [20] as

$$\alpha + (d-1)\beta = 0, \quad \beta + (d-1)\delta + 2\epsilon = 0. \quad (3.21)$$

We rewrite the two-point function of stress tensors into more familiar form

$$\langle T_{ij}^{(m)}(x) T_{kl}^{(m)}(x') \rangle = C_T^\phi \left(\frac{\mathcal{I}_{ij,kl}(s)}{s^{2d}} + c_r^2 \frac{\bar{\mathcal{I}}_{ij,kl}(\bar{s})}{\bar{s}^{2d}} + c_r \frac{\#_{ij,kl}}{(s\bar{s})^d} \right), \quad (3.22)$$

$$\langle T_{ij}^{(m)}(x) T_{kl}^{(n)}(x') \rangle = C_T^\phi \left(c_t^2 \frac{\bar{\mathcal{I}}_{ij,kl}(\bar{s})}{\bar{s}^{2d}} \right), \quad C_T^\phi = \frac{\kappa^2 d}{d-1}, \quad (3.23)$$

where the first term of (3.22) agrees with that of a CFT. We have

$$\mathcal{I}_{ij,kl}(s) = \frac{1}{2} (I_{ik}(s)I_{jl}(s) + I_{il}(s)I_{jk}(s)) - \frac{1}{d} \delta_{ij} \delta_{kl} \quad (3.24)$$

$$\bar{\mathcal{I}}_{ij,kl}(\bar{s}) = \mathcal{I}_{ij,kl}(s)|_{x' \rightarrow \bar{x}'}, \quad (3.25)$$

and $\#_{ij,kl}/(s\bar{s})^d$ comes from the mix of the CFT term s and its mirror term \bar{s} . It is worth mentioning that $\#_{na,kl}$ vanish in the limit $x \rightarrow 0$. In such limit, we have $1 - c_r^2 = (p-1)c_t^2$ and can verify that the constraint (3.9) on the node. Recall that we have $c_r = -\frac{p-2}{p}$, $c_t = \frac{2}{p}$ and $\gamma(v)$ is given by (3.18,3.20).

3.2.2 Maxwell theory

The Euclidean action of 4-dimensional Maxwell theory reads

$$I = \frac{1}{4} \sum_{m=1}^p \int_{E_m} d^4x F_{ij}^{(m)} F^{ij}, \quad (3.26)$$

whose variations yields

$$\delta I|_N = \sum_{m=1}^p \int_N d^3y F^{na(m)} \delta A_a = 0. \quad (3.27)$$

From the above action variations, we read off the JC

$$\text{vector JC: } \sum_{m=1}^p F^{na(m)}|_N = 0, \quad F_{ab}|_N = F_{ab}^{(n)}|_N. \quad (3.28)$$

We remark that the second term of (3.28) is the gauge invariant expression of the continuity condition $A_a^{(m)} = A_a^{(n)}$. Given the stress tensor

$$T_{ij} = F_{ik} F_j^k - \frac{1}{4} \delta_{ij} F_{kl} F^{kl}, \quad (3.29)$$

it is easy to see that the vector JC (3.28) yields the conservation law (3.13) on the node.

In the Feynman gauge, the vector two-point function obeying JC (3.28) becomes

$$\langle A_1(x)A_1(x') \rangle = \frac{\kappa}{2} \cdot \begin{cases} \frac{1-c_r v_I^2}{|x^{(m)} - x'^{(m)}|^2}, & \text{same edge,} \\ \frac{-c_t}{|x^{(m)} - x'^{(n)}|^2}, & \text{mixed edge,} \end{cases} \quad (3.30)$$

and

$$\langle A_a(x)A_b(x') \rangle = \frac{\kappa \delta_{ab}}{2} \cdot \begin{cases} \frac{1+c_r v_I^2}{|x^{(m)} - x'^{(m)}|^2}, & \text{same edge,} \\ \frac{c_t}{|x^{(m)} - x'^{(n)}|^2}, & \text{mixed edge,} \end{cases} \quad (3.31)$$

which yields the two-point function of F_{ij}

$$\begin{aligned} \langle F_{ij}(x)F_{kl}(x') \rangle = & \frac{1}{s^4} [2a(v)(I_{ik}I_{jl} - I_{il}I_{jk}) \\ & + b(v) \left(\hat{X}_i \hat{X}'_k I_{jl} - \hat{X}_j \hat{X}'_k I_{il} - \hat{X}_i \hat{X}'_l I_{jk} + \hat{X}_j \hat{X}'_l I_{ik} \right)], \end{aligned} \quad (3.32)$$

with

$$a(v_I) = \kappa(1 + c_r v_I^4), \quad b(v_I) = -4\kappa c_r v_I^4, \quad (3.33)$$

for the same edge and

$$a(v_{II}) = \kappa c_t, \quad b(v_{II}) = 0, \quad (3.34)$$

for the mixed edge. Recall that $x' = (x', y'_a)$ of I_{ik} , \hat{X}_i , \hat{X}'_k should be replaced with $\bar{x}' = (-x', y'_a)$ in the mixed edge. From (3.32) and (3.29), we obtain the two-point functions of stress tensors (3.6) for Maxwell theory with

$$\alpha(v_I) = 12\kappa^2 (1 + c_r^2 v_I^8), \quad \gamma(v_I) = -8\kappa^2 (1 - c_r^2 v_I^8), \quad \epsilon(v_I) = 8\kappa^2 (1 + c_r^2 v_I^8), \quad (3.35)$$

for the same edge and

$$\alpha(v_{II}) = 12\kappa^2 c_t^2, \quad \gamma(v_{II}) = -8\kappa^2 c_t^2, \quad \epsilon(v_{II}) = 8\kappa^2 c_t^2, \quad (3.36)$$

for the mixed edge. From the above equations together with (3.16), we verify the consistent condition (3.9) is obeyed. Finally, we rewrite the the two-point functions of stress tensors into more more familiar form

$$\langle T_{ij}^{(m)}(x) T_{kl}^{(m)}(x') \rangle = C_T^A \left(\frac{\mathcal{I}_{ij,kl}(s)}{s^8} + c_r^2 \frac{\bar{\mathcal{I}}_{ij,kl}(\bar{s})}{\bar{s}^8} \right), \quad (3.37)$$

$$\langle T_{ij}^{(m)}(x) T_{kl}^{(n)}(x') \rangle = C_T^A \left(c_t^2 \frac{\bar{\mathcal{I}}_{ij,kl}(\bar{s})}{\bar{s}^8} \right), \quad C_T^A = 16\kappa^2. \quad (3.38)$$

Interestingly, unlike the scalar, there are no cross-terms in $\langle TT \rangle$ for a vector.

3.2.3 Dirac fermions

The Euclidean action of free Dirac field reads in flat space

$$I = \int d^d x \bar{\psi} (\gamma^i \overleftrightarrow{\nabla}_i) \psi \quad (3.39)$$

$$= \frac{1}{2} \sum_m \int_{E_m} d^d x (\bar{\psi} \gamma^i \partial_i \psi - (\partial_i \bar{\psi}) \gamma^i \psi), \quad (3.40)$$

where γ^i satisfies the the Clifford algebra in Euclidean signature

$$\{\gamma_i, \gamma_j\} = 2\delta_{ij}. \quad (3.41)$$

Following [20], we define the projectors Π_- and Π_+

$$\Pi_{\pm} = \frac{1}{2} (\mathbf{1} \pm U), \quad (3.42)$$

where $\chi = \Pi_+ - \Pi_-$ obeys

$$U\gamma_1 = -\gamma_1\bar{U}, \quad U\gamma_a = \gamma_a\bar{U}, \quad U^2 = \bar{U}^2 = \mathbf{1}. \quad (3.43)$$

The current and stress tensor for Dirac fields read

$$J^i = i\bar{\psi}\gamma^i\psi, \quad (3.44)$$

$$\begin{aligned} T_{ij} &= \bar{\psi}\gamma_{(i}\overleftrightarrow{\nabla}_{j)}\psi \\ &= \frac{1}{2} (\partial_{(i}\bar{\psi}\gamma_{j)}\psi - \bar{\psi}\gamma_{(i}\partial_{j)}\psi). \end{aligned} \quad (3.45)$$

To satisfy the conservation law $\sum_m^{(m)} J_n = \sum_m^{(m)} T_{na} = 0$ on the node, we choose the following JC

$$\sum_m \Pi_- \psi|_N = \sum_m \bar{\psi} \bar{\Pi}_-|_N = 0, \quad \Pi_+ \psi|_N = \Pi_+ \bar{\psi}|_N, \quad \bar{\psi} \bar{\Pi}_+|_N = \bar{\psi} \bar{\Pi}_+|_N, \quad (3.46)$$

where $\bar{\Pi}_{\pm} = \frac{1}{2} (\mathbf{1} \pm \bar{\chi})$. The two-point function of Dirac field satisfying the above JC is given by

$$\langle \psi(x) \bar{\psi}(x') \rangle = \kappa \cdot \begin{cases} \frac{\gamma \cdot (\frac{x-x'}{|x-x'|^d}) + c_r \frac{\gamma \cdot (\frac{x-x'}{|x-x'|^d}) \bar{U}}{|x-x'|^d}, & \text{same edge,} \\ c_t \frac{\gamma \cdot (\frac{x-x'}{|x-x'|^2}) \bar{U}}{|x-x'|^2}, & \text{mixed edge,} \end{cases} \quad (3.47)$$

where $(\frac{x}{|x} - \frac{x'}{|x'}) = (x+x', y_a - y'_a)$. Then, we derive the two-point functions of stress tensors

$$\langle T_{ij}(x) T_{kl}(x') \rangle = C_T^\psi \left(\frac{\mathcal{I}_{ij,kl}(s)}{s^{2d}} + c_r^2 \frac{\bar{\mathcal{I}}_{ij,kl}(\bar{s})}{\bar{s}^{2d}} \right), \quad (3.48)$$

$$\langle T_{ij}(x) T_{kl}(x') \rangle = C_T^\psi \left(c_t^2 \frac{\bar{\mathcal{I}}_{ij,kl}(\bar{s})}{\bar{s}^{2d}} \right), \quad C_T^\psi = \frac{d\kappa^2 \text{tr}(\mathbf{1})}{2}, \quad (3.49)$$

where $\text{tr}(\mathbf{1}) = 2^{\lfloor d/2 \rfloor}$. In the expressions of (3.6), we have

$$\alpha(v_I) = \frac{d-1}{2} \kappa^2 \text{tr}(\mathbf{1}) \left(1 + c_r^2 v_I^{2d}\right), \quad \gamma(v_I) = -\frac{d}{4} \kappa^2 \text{tr}(\mathbf{1}) \left(1 - c_r^2 v_I^{2d}\right), \quad \epsilon(v_I) = \frac{d}{4} \kappa^2 \text{tr}(\mathbf{1}) \left(1 + c_r^2 v_I^{2d}\right), \quad (3.50)$$

for the same edge and

$$\alpha(v_{II}) = \frac{(d-1)}{2} \kappa^2 \text{tr}(\mathbf{1}) c_t^2, \quad \gamma(v_{II}) = -\frac{d}{4} \kappa^2 \text{tr}(\mathbf{1}) c_t^2, \quad \epsilon(v_{II}) = \frac{d}{4} \kappa^2 \text{tr}(\mathbf{1}) c_t^2, \quad (3.51)$$

for the mixed edge.

3.3 Holographic theories

This subsection investigates the two-point function of stress tensors in AdS/NCFT with a tensionless Net-brane. Following [22], we take the ansatz for the metric perturbations as

$$ds^2 = \frac{dz^2 + dx^2 + \delta_{ab} dy^a dy^b + H_{\mu\nu} dx^\mu dx^\nu}{z^2}, \quad (3.52)$$

with the gauge

$$H_{zz}(z=0, \mathbf{x}) = H_{zi}(z=0, \mathbf{x}) = 0. \quad (3.53)$$

Imposing the JC (1.4, 1.5) on the tensionless Net-brane and the DBC

$$H_{ij}(z=0, \mathbf{x}) = \hat{H}_{ij}(\mathbf{x}), \quad (3.54)$$

on the AdS boundary, we obtain the linear metric perturbations

$$\begin{aligned} \overset{(m)}{H}_{\mu\nu}(z, \mathbf{x}) = & \frac{C_T}{2d} \left\{ \int_{E_m} d^d x' \left[\frac{z^d}{S^{2d}} J_{\mu i} J_{\nu j} P_{ijkl} + c_r \frac{z^d}{\bar{S}^{2d}} \bar{J}_{\mu i} \bar{J}_{\nu j} P_{ijkl} \right] \hat{H}_{kl}(\mathbf{x}') \right. \\ & \left. + \sum_{n \neq m} c_t \int_{E_n} d^d x' \frac{z^d}{\bar{S}^{2d}} \bar{J}_{\mu i} \bar{J}_{\nu j} P_{ijkl} \hat{H}_{kl}(\mathbf{x}') \right\}, \end{aligned} \quad (3.55)$$

where

$$\begin{aligned} C_T &= \frac{2\Gamma[d+2]}{\pi^{d/2} \Gamma[d/2] (d-1)}, \\ S^2 &= z^2 + (x-x')^2 + (y_a - y'_a)^2, \\ \bar{S}^2 &= z^2 + (x+x')^2 + (y_a - y'_a)^2, \\ P_{ijkl} &= \frac{1}{2} (\delta_{ik} \delta_{jl} + \delta_{il} \delta_{jk}) - \frac{1}{d} \delta_{ij} \delta_{kl}, \\ J_{\mu\nu} &= \delta_{\mu\nu} - 2 \frac{(x_\mu - x'_\mu)(x_\nu - x'_\nu)}{S^2}, \\ \bar{J}_{\mu\nu} &= J_{\mu\nu} - 2X_\mu X'_\nu, \end{aligned} \quad (3.56)$$

and

$$X_\mu = \frac{1}{S\bar{S}} (2xz, x^2 - x'^2 - (y_a - y'_a)^2 - z^2, 2x(y_a - y'_a)), \quad (3.57)$$

$$\bar{X}_\mu = \frac{1}{S\bar{S}} (-2x'z, x'^2 - x^2 - (y_a - y'_a)^2 - z^2, 2x'(y_a - y'_a)). \quad (3.58)$$

According to [22], the on-shell quadratic action for H_{ij} is given by

$$\begin{aligned} I_2 &= \sum_m \int_{E_m} d^d x z^{1-d} \left(\frac{1}{4} H_{ij} \partial_z H_{ij} - \frac{1}{2} H_{ij} \partial_j H_{zi} \right) \\ &= \frac{C_T}{8} \left\{ \sum_m \int_{E_m} d^d x d^d x' \hat{H}_{ij}(x) \left[\frac{\mathcal{I}_{ij,kl}}{s^{2d}} + c_r \frac{\bar{\mathcal{I}}_{ij,kl}}{\bar{s}^{2d}} \right] \hat{H}_{kl}(x') \right. \\ &\quad \left. + \sum_m \sum_{n \neq m} \int_{E_m} \int_{E_n} d^d x d^d x' \hat{H}_{ij}(x) c_t \frac{\bar{\mathcal{I}}_{ij,kl}}{\bar{s}^{2d}} \hat{H}_{kl}(x') \right\}, \end{aligned} \quad (3.59)$$

where

$$\mathcal{I}_{ij,kl} = \lim_{z \rightarrow 0} \frac{1}{2} (J_{ik} J_{jl} + J_{il} J_{jk}) - \frac{1}{d} \delta_{ij} \delta_{kl}, \quad (3.60)$$

$$\bar{\mathcal{I}}_{ij,kl} = \lim_{z \rightarrow 0} \frac{1}{2} (\bar{J}_{ik} \bar{J}_{jl} + \bar{J}_{il} \bar{J}_{jk}) - \frac{1}{d} \delta_{ij} \delta_{kl}. \quad (3.61)$$

From (3.59), we obtain the holographic two-point function of stress tensor

$$\langle T_{ij}^{(m)}(x) T_{kl}^{(m)}(x') \rangle = C_T \left(\frac{\mathcal{I}_{ij,kl}(s)}{s^{2d}} + c_r \frac{\bar{\mathcal{I}}_{ij,kl}(\bar{s})}{\bar{s}^{2d}} \right), \quad (3.62)$$

$$\langle T_{ij}^{(m)}(x) T_{kl}^{(n)}(x') \rangle = C_T \left(c_t \frac{\bar{\mathcal{I}}_{ij,kl}(\bar{s})}{\bar{s}^{2d}} \right). \quad (3.63)$$

We remark that (3.62) agrees with that of AdS/BCFT [23] for $p = 1$ and $c_r = (2-p)/p = 1$, which is a test of our calculations. Finally, we rewrite the above equations into the form of (3.6) with

$$\alpha(v_I) = \frac{(d-1)}{d} C_T (1 + c_r v_I^{2d}), \quad \gamma(v_I) = -\frac{C_T}{2} (1 - c_r v_I^{2d}), \quad \epsilon(v_I) = \frac{C_T}{2} (1 + c_r v_I^{2d}), \quad (3.64)$$

for same edge and

$$\alpha(v_{II}) = \frac{(d-1)}{d} C_T c_t, \quad \gamma(v_{II}) = -\frac{C_T}{2} c_t, \quad \epsilon(v_{II}) = \frac{C_T}{2} c_t, \quad (3.65)$$

for mixed edge. We verify that they obey the constraints (3.9) from energy conservation.

In summary, we have examined the general form of two-point functions for NCFTs. They share similar expressions with BCFTs but involve more independent functions. We also explored examples of free theories and the AdS/NCFT with tensionless branes.

4 Holographic entanglement entropy

This section investigates holographic entanglement entropy (HEE) in AdS/NCFT. We propose that the RT surface connect solely to the Net-brane for a connected subsystem within the network. We derive the junction condition for Ryu-Takayanagi (RT) surfaces and confirm that our proposal is consistent with the strong subadditivity of entanglement entropy. Lastly, we explore several natural proposals for network entropy and analyze their behaviors under node RG flow.

4.1 General theories

Let's analyze the simplest network consisting of three edges connected by a single node. There are two natural proposals regarding the entanglement entropy (HEE) of a connected subsystem that includes the node within this network. See Fig. 4. The first proposal, based on the AdS/BCFT framework, suggests that the RT surfaces are perpendicular to the Net-brane and may be disconnected. The second proposal, however, asserts that all RT surfaces must be interconnected through the same interaction on the Net-brane. While the first proposal leads to a smaller HEE, the second approach is ultimately the correct one for the following reasons.

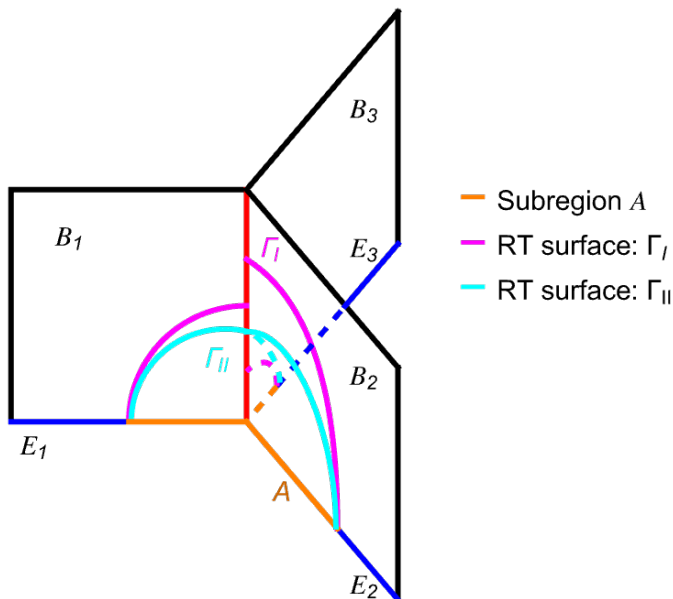


Figure 4: Two proposals of RT surfaces. The orange lines illustrate a typical choice for the subregion A . The magenta curves, Γ_I , represent the RT surfaces from the first proposal, which is discontinuous at the Net-brane and intersects it orthogonally. In contrast, the cyan-blue curves Γ_{II} correspond to the second proposal, where the RT surfaces are continuous across the Net-brane but not necessarily orthogonal to it.

- Naturally, a connected subsystem of NCFT corresponds to a connected RT surface in bulk. It is essential to note that a network node differs from a boundary; information

and energy can pass through a node and flow into different network edges. Consequently, the Net-brane dual to a node is a link rather than the end of spacetime. Therefore, physical continuity necessitates the presence of a connected RT surface in the bulk.

- AdS/ICFT (interface CFT) is a specific case of AdS/NCFT that involves only two edges and one node. When considering AdS/ICFT with a tensionless brane, it reduces to the standard AdS/CFT. In this context, the corresponding RT surface should be connected as in AdS/CFT. It indisputably rules out the disconnected proposal for HEE in AdS/NCFT.
- The second proposal of HEE obeys the strong subadditivity of entanglement entropy. Let's consider two subsystems, A_a (shown with orange lines) and A_b (shown with green lines), along with their corresponding RT surfaces, Γ_a and Γ_b , as depicted in Fig. 5a. By combining these RT surfaces, we obtain the extremal surfaces $\tilde{\Gamma}_\cup$ and $\tilde{\Gamma}_\cap$ for the combined subsystems $A_a \cup A_b$ and the intersection $A_a \cap A_b$, illustrated in Fig. 5b. Since RT surfaces are minimal, their areas are less than those of the extremal surfaces $\tilde{\Gamma}_\cup$ and $\tilde{\Gamma}_\cap$, which equals the total areas of Γ_a and Γ_b . In this way, we prove subadditivity in AdS/NCFT

$$S(A_a) + S(A_b) = \frac{\text{Area}_{\tilde{\Gamma}_\cup} + \text{Area}_{\tilde{\Gamma}_\cap}}{4G_N} \geq S(A_a \cup A_b) + S(A_a \cap A_b). \quad (4.1)$$

- Last but not least, only the second proposal aligns with the monotonicity of entanglement entropy for networks containing internal edges. Consider a finite subregion A that includes at least two nodes and one internal edge within an infinite network. When we increase the length of the internal edge or add more internal edges, the entanglement between these edges and the complement \bar{A} increases. Consequently, the entanglement entropy should also rise with the length or number of internal edges. It holds for the second proposal of HEE, which we will demonstrate below. In contrast, for the first proposal, the disconnected RT surface associated with the internal edge approaches infinity in the bulk, resulting in zero area. Therefore, the corresponding HEE is irrelevant to the length or number of internal edges, which is unphysical.

Let's prove that the second proposal of HEE increases when we add a new internal edge to the connected subsystem A . Without loss of generality, we focus on the Poincaré AdS with tensionless Net-branes in bulk. We also assume that the subsystem A is much smaller than its complement \bar{A} . We can simplify this problem by considering the opposite scenario: removing an internal edge. Label the network with p internal edges and the corresponding HEE as $\text{Net}(p)$ and $S(p)$. When we remove one internal edge while keeping the RT surfaces of the other edges the same, the areas of the extremal surfaces $S_0(p-1)$ decrease. Thus, we have $S(p) > S_0(p-1)$. It's important to note that $S_0(p-1)$ is not the same as the HEE $S(p-1)$ for the network $\text{Net}(p-1)$, because the RT surfaces can

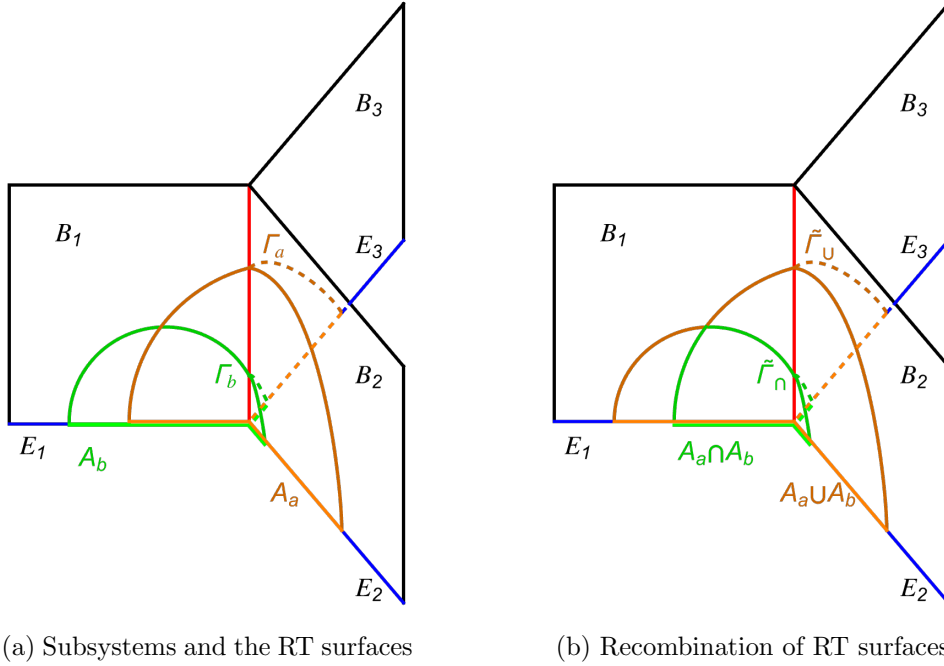


Figure 5: Left: subsystems A_a (orange lines) and A_b (green lines) on edges and the corresponding RT surfaces Γ_a (orange curves) and Γ_b (green curves) in bulk. Right: subsystems $A_a \cup A_b$ (orange lines) and $A_a \cap A_b$ (green lines) and the corresponding extremal surfaces $\tilde{\Gamma}_U$ (orange curves) and $\tilde{\Gamma}_\cap$ (green curves), which combines the RT surfaces of Γ_a and Γ_b .

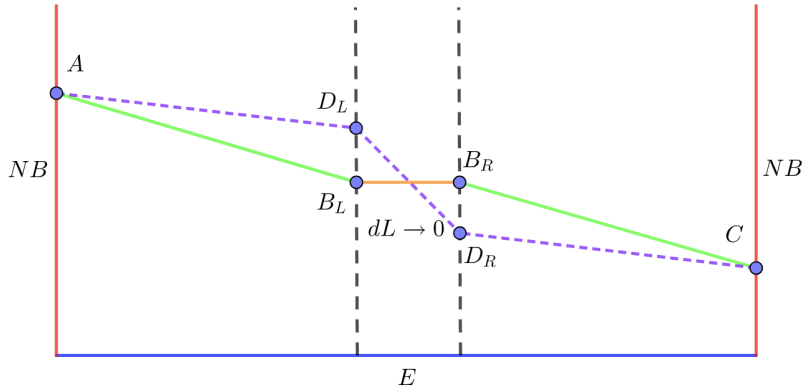


Figure 6: When we increase the edge length by $dL \rightarrow 0$ (represented by the orange line), the RT surface transitions from the green curves $AB_L \cup B_R C$ to the purple dashed curves $AD_L \cup D_L D_R \cup D_R C$.

change between $\text{Net}(p)$ and $\text{Net}(p-1)$. Since RT surfaces are minimal, we generally have $S_0(p-1) \geq S(p-1)$. It leads us to prove the inequality

$$S(p) > S(p-1). \quad (4.2)$$

We will demonstrate that the HEE increases when the internal edge is slightly extended

by a length dL . In Fig. 6, the change is illustrated, focusing on Poincaré AdS for simplicity. When we increase the edge length by $dL \rightarrow 0$ (represented by the orange line), the RT surface transitions from the green curves $AB_L \cup B_R C$ to the purple dashed curves $AD_L \cup D_L D_R \cup D_R C$. Since dL is very small, the local region around $D_L D_R$ can be treated as flat space if we ignore second-order corrections $O(dL^2)$. Thus, we can write

$$\text{Area}(D_L D_R) > \text{Area}(D_L B_L \cup D_R B_R), \quad (4.3)$$

in the linear order of dL . Similarly, we have near the local regions of $D_L B_L$ and $D_R B_R$ that

$$\text{Area}(AD_L \cup D_L B_L) > \text{Area}(AB_L), \quad \text{Area}(CD_R \cup D_R B_R) > \text{Area}(CB_R). \quad (4.4)$$

Combining these inequalities, we find

$$\begin{aligned} \text{Area}(AD_L \cup D_L D_R \cup D_R C) &> \text{Area}(AD_L \cup D_R C) + \text{Area}(D_L B_L \cup D_R B_R) \\ &> \text{Area}(AB_L \cup B_R C), \end{aligned} \quad (4.5)$$

which confirms that the HEE indeed increases with an increase in internal edge length.

From now on, we will focus on the correct proposal for HEE involving connected RT surfaces on the Net-brane. We aim to analyze how these RT surfaces are interconnected on a single Net-brane. We obtain the following connecting condition

$$\sum_{m=1}^p (n)_\alpha^{(m)} \frac{\partial x^\mu}{\partial \xi^\alpha} \frac{\partial x^\nu}{\partial y^i} g_{\mu\nu} |_{\Gamma \cap \text{NB}} = 0, \quad (4.6)$$

where $(n)_\alpha^{(m)}$ are the unit vectors normal to the intersection $\gamma = \Gamma \cap \text{NB}$ directed along the RT surface Γ of branch B_m approaching the Net-brane NB, x^μ , ξ^α and y^i are the coordinates of the bulk, the RT surfaces Γ and Net-brane NB, respectively. It is important to note that the AdS/NCFT simplifies to AdS/BCFT under the Z_p symmetry. Under this condition, the connecting condition (4.6) reduces to the orthogonality condition for the RT surface and EOW brane in AdS/BCFT. It can be regarded as a test of our result (4.6).

Similar to the junction condition for bulk branches, the connecting condition for RT surfaces can be derived from the variational principle. See [17] for a similar case in AdS/ICFT. We label the embedding function of RT surfaces as $x^\mu(\xi^\alpha)$ and get the induced metric on the RT surface Γ as follows

$$h_{\Gamma \alpha\beta} = \frac{\partial x^\mu}{\partial \xi^\alpha} \frac{\partial x^\nu}{\partial \xi^\beta} g_{\mu\nu}. \quad (4.7)$$

The area of the RT surface is given by

$$A = \int_{\Gamma} d^{d-1} \xi \sqrt{h_{\Gamma}}. \quad (4.8)$$

Taking variations of this area functional with respect to x^μ and integrating by parts, we obtain

$$\delta A = - \int_{\Gamma} d^{d-1} \xi \sqrt{h_{\Gamma}} K_{\Gamma \mu} \delta x^\mu + \int_{\gamma} d^{d-2} y \sqrt{h_{\gamma}} \sum_m (n)_\alpha^{(m)} \frac{\partial x^\mu}{\partial \xi^\alpha} g_{\mu\nu} \delta x^\nu = 0, \quad (4.9)$$

where $K_{\Gamma \mu}$ represents the trace of the extrinsic curvatures from the bulk to the RT surface, and $\gamma = \Gamma \cap \text{NB}$ denotes the interaction between the RT surface Γ and the Net-brane NB . The extrinsic curvature is defined by

$$K_{\Gamma \alpha\beta}^{\mu} = \partial_{\alpha} \partial_{\beta} x^{\mu} - \gamma_{\alpha\beta}^{\gamma} \partial_{\gamma} x^{\mu} + \Gamma_{\sigma\rho}^{\mu} \partial_{\alpha} x^{\sigma} \partial_{\beta} x^{\rho}, \quad (4.10)$$

where $\gamma_{\alpha\beta}^{\gamma}$ and $\Gamma_{\sigma\rho}^{\mu}$ are the Levi-Civita connections with respect to $h_{\alpha\beta}$ and $g_{\mu\nu}$, respectively. The bulk term of (4.9) indicates that the RT surface is a minimal surface with

$$K_{\Gamma \mu} = 0. \quad (4.11)$$

Furthermore, since $\delta x^{\mu}|_{\gamma} = (\partial x^{\mu} / \partial y^i) \delta y^i$ is defined along the Net-brane, the boundary term of (4.9) gives us the connecting condition (4.6) for the RT surfaces.

4.2 Network entropy

This subsection discusses holographic entanglement entropy for networks. Let us start with the simplest network, which has p edges linked by a single node. The vacuum of this network is dual to Poincaré AdS (2.16, 2.17). For simplicity, we focus on AdS₃ and choose the subsystem as $A : x \leq L_m$. The embedding function of RT surface reads [10]

$$z^2 + \left(x - \binom{(m)}{a} \right)^2 = \binom{(m)}{b}^2, \quad (4.12)$$

where $\binom{(m)}{a}$, $\binom{(m)}{b}$ are free parameters. Substituting typical points $(0, L_m)$ and (z_b, x_b) into the above embedding function, we determine the parameters $\binom{(m)}{a}$, $\binom{(m)}{b}$ and drive the area of RT surface

$$A = \sum_{m=1}^p \log \left(\frac{(L_m - x_b)^2 + z_b^2}{z_b \epsilon} \right), \quad (4.13)$$

ϵ labels the UV cut-off of z , and (z_b, x_b) denotes the common intersection point of RT surfaces on the Net-brane. According to (2.17), we have $x_b = -\sinh(\rho)z_b$. By minimizing the area (4.13), we can determine z_b . For the symmetric case $L_m = L$, we have $z_b = L \text{sech}(\rho)$, yielding

$$A|_{L_m=L} = p \log \left(\frac{2L}{\epsilon} \right) + p\rho. \quad (4.14)$$

From (4.13), we read off the universal logarithmic divergent term of entanglement entropy

$$S_{\text{EE}} = \frac{A}{4G_N} = \frac{cp}{6} \log \left(\frac{1}{\epsilon} \right) + \text{finite terms}, \quad (4.15)$$

where $c = 3l/2G_N$ is the central charge, p is the number of edges. Note that we have set the AdS radius $l = 1$ in AdS₃.

Let us go on to analyze the finite terms, which include the network information. There are several natural ways to extract the network contributions to entanglement entropy. We

define the type I network entropy as the difference between the entanglement entropy of NCFT and CFT

$$S_I = S_{EE} - S_{\text{CFT}}, \quad (4.16)$$

where S_{CFT} is half the entanglement entropy of a strip with the width $2L_m$

$$S_{\text{CFT}} = \frac{c}{6} \sum_{m=1}^p \log \left(\frac{2L_m}{\epsilon} \right). \quad (4.17)$$

For the symmetric case $L_m = L$, we get

$$S_I|_{L_m=L} = \frac{cp}{6} \rho, \quad (4.18)$$

which increases with the brane tension (2.18). According to [18], we have $\rho_{\text{UV}} \geq \rho_{\text{IR}}$ under boundary RG flow. The case for the network node is similar. Thus, similar to the boundary entropy, the type I network entropy decreases under the renormalization group (RG) flow

$$S_I|_{\text{IR}} \leq S_I|_{\text{UV}}. \quad (4.19)$$

It should be stressed that (4.19) also holds for the asymmetric case $L_i \neq L_j$. See Fig. 8 for an example.

Inspired by the boundary entropy in AdS/BCFT, we propose another natural definition of network entropy

$$S_{\text{II}} = S_{EE}(\rho) - S_{EE}(0), \quad (4.20)$$

which we refer to as type II network entropy. Note that S_{CFT} represents the disconnected HEE proposal of sect. 4.1 with $\rho = 0$, which is smaller than the connected HEE proposal $S_{EE}(\rho = 0)$. Consequently, we have the following inequality

$$S_{\text{II}} \leq S_I, \quad (4.21)$$

where this inequality is saturated in the symmetric case $L_m = L$. Similar to S_I , the type II network entropy S_{II} increases with the brane tension, adhering to the RG flow relation

$$S_{\text{II}}|_{\text{IR}} \leq S_{\text{II}}|_{\text{UV}}. \quad (4.22)$$

See Fig. 8 for an example.

The entropy difference between NCFT and BCFT defines the type III network entropy

$$S_{\text{III}} = S_{EE} - S_{\text{BCFT}}, \quad (4.23)$$

where S_{BCFT} is given by the area of extremal surfaces normal to the Net-brane

$$S_{\text{BCFT}} = \frac{cp}{6} \rho + \frac{c}{6} \sum_{m=1}^p \log \left(\frac{2L_m}{\epsilon} \right). \quad (4.24)$$

It is the first proposal of HEE discussed in sect.4.1. Since S_{BCFT} is defined by the area of minimal surfaces ending on the Net-brane, not necessarily intersecting at a single point as S_{EE} , we have $S_{\text{BCFT}} \leq S_{\text{EE}}$. As a result, the type III network entropy is semi-positive definite

$$S_{\text{III}} \geq 0. \quad (4.25)$$

Note that $S_{\text{III}} = 0$ for the symmetric case $L_m = L$. Let us discuss the physical meanings of type III network entropy more. As discussed in sect. 2.3, the spectrum of NCFTs consists of isolated modes (AdS/BCFT with NBC) and transparent modes (AdS/BCFT with DBC/CBC). The entanglement entropy of isolated modes at each edge is represented by S_{BCFT} . Thus, S_{III} characterizes the entanglement between NCFT modes, excluding those from isolated modes. Given this interpretation, it follows naturally that S_{III} is non-negative.

Unlike S_{I} and S_{II} , the type III network entropy S_{III} decreases with increasing ρ (see Fig. 8). Thus, it does not reflect the degrees of freedom at the nodes. Instead, it effectively describes the network's structure and size, including the lengths and the number of internal edges. To illustrate this, we consider Poincaré AdS₃ with tensionless Net-branes as an example. For a network consisting of two nodes, four external edges, and p internal edges, the expression for the type III network entropy S_{III} is given by:

$$S_{\text{III}} = \frac{c}{6} \left[2p \tanh^{-1} \left(\sqrt{\frac{L_2^2}{4z_b^2 + L_2^2}} \right) + 4 \log \left(\frac{z_b^2 + L_1^2}{2L_1 z_b} \right) \right], \quad (4.26)$$

where L_1 and L_2 are the lengths of connected subsystem A on the external and internal edges, respectively. The interaction z_b of the RT surfaces on the Net-brane can be determined numerically by minimizing the equation above. We have numerically verified that S_{III} increases with the length L_2 and the number p of internal edges (see Fig. 7). As discussed around eqs. (4.2,4.5), S_{EE} increases with the lengths and number of internal edges, while S_{BCFT} is independent of the internal edges. Consequently, the monotonic increase of S_{III} concerning edge length always holds.

To end this section, we draw various network entropies in Fig. 8. It shows S_{I} and S_{II} increase with brane tension, while S_{III} decreases with brane tension. Besides, $S_{\text{I}} = S_{\text{III}}$ at $\rho = 0$, $S_{\text{I}} \geq S_{\text{II}}$ and $S_{\text{III}} \geq 0$.

5 Holographic network problems

This section provides a brief discussion of famous network and graph problems from a holographic perspective. We use the shortest path problem as an example and reserve the study of other famous network and graph problems for future work. The shortest path problem seeks to determine the shortest path from a starting point to an ending point within a network. For example, calculate the shortest driving route in the urban road network from one place to another. Dijkstra's algorithm is a classic algorithm for solving this problem.

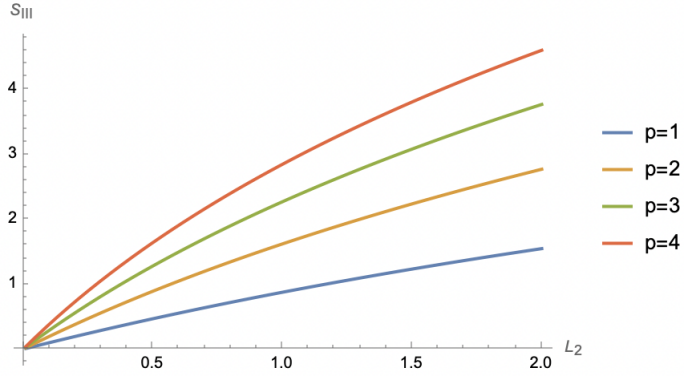


Figure 7: The type III network entropy increases with the length L_2 and number p of internal edges. Here we have set length of external edge $L_1 = 1$ and $c/6 = 1$. The blue, orange, green and red curves corresponds to $p = 1, 2, 3, 4$, respectively.

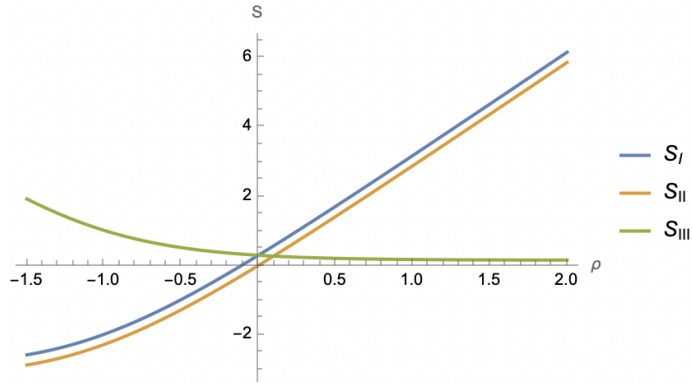


Figure 8: Various network entropies vary with the brane tension $T = p(d-1) \tanh \rho$. We choose $L_1 = 1, L_2 = 2, L_3 = 3$ and set $c/6 = 1$. The blue, orange, and green curves denote S_I, S_{II} and S_{III} , respectively. It shows S_I and S_{II} increase with ρ , while S_{III} decreases with ρ . Besides, $S_I = S_{III}$ at $\rho = 0$, $S_I \geq S_{II}$ and $S_{III} \geq 0$.

Consider a one-dimensional Euclidean network with n nodes N and p edges E_m of length L_m . Each edge E_m is dual to an AdS_2 spacetime or a time slice of AdS_3 in the bulk branch B_m

$$d^{(m)_2} s = \frac{dz^2 + d^{(m)_2} x^2}{z^2}, \quad 0 \leq x \leq L_m, \quad (5.1)$$

where the nodes are located at $z = 0, x = 0, L_m$. We glue the branch B_m with tensionless Net-branes to get the gravity dual of the network. The network generally allows multiple paths from the starting point A to the endpoint B . The paths must not contain loops to ensure they are the shortest routes. Consider an arbitrary path p_l that traverses the edge $\mathcal{E}_l = \{E_i | E_i \cap p_l \neq \emptyset\}$. This edge set \mathcal{E}_l selects a branch set $\mathcal{B}_l = \{B_i | B_i \cap \mathcal{E}_l \neq \emptyset\}$ in the bulk. Since the path p_l is loop-free, the branch set \mathcal{B}_l is also loop-free. In other words,

each branch connects to at most one branch on the Net-brane in the set \mathcal{B}_l . Since the Net-branes are tensionless, the branch set \mathcal{B}_l can be viewed as a smooth AdS₂ spacetime without Net-branes. The geodesic distance connecting points A and B in AdS₂ is given by

$$L_{AB} = 2 \log\left(\frac{l_{AB}}{\epsilon}\right), \quad (5.2)$$

which increases monotonically with the distance l_{AB} between points A and B in \mathcal{E}_l . Here ϵ is the UV cut-off of z . Thus, minimizing the distance l_{AB} on the network is equivalent to minimizing the distance L_{AB} in the bulk. In AdS/CFT, the two-point function of local operators dual to massive particles is determined by the proper distance in bulk

$$\langle O(A)O(B) \rangle \sim e^{-ML_{AB}}, \quad (5.3)$$

where M denotes the particle mass. Thus, from the holographic perspective, the shortest path problem of the network is dual to the shortest geodesic problem in bulk and is also equivalent to minimizing the holographic two-point correlators of massive operators⁶.

We consider a variation of the shortest path problem where nodes in the network have weights, such as toll stations. Each time you pass through a toll station N_i , you incur a cost of c_i . The goal is to find the most economical route from point A to point B, minimizing the total price, including fuel and toll fees. The total cost can be expressed as $(\lambda l_{AB} + \sum_{N_i \in p_l} c_i)$, where λ is the fuel cost per distance, l_{AB} is the length of the journey, and p_l is the path from A to B. To simplify this problem, we can convert it into a standard shortest path problem by redefining the length between two nodes N_i and N_j : $\bar{L}_{ij} = L_{ij} + \frac{c_i + c_j}{2\lambda}$. This way, minimizing the new length \bar{L}_{AB} will also minimize the total costs effectively.

In summary, we examined the holographic shortest path problem for networks and its variant. It is equivalent to finding the shortest distance in bulk or the holographic two-point correlators for massive operators. While the holographic approach does not simplify the original shortest path problem, it could offer new insights into specific network issues. We will explore this intriguing problem in future research.

6 Conclusions and Discussions

This paper explores the network conformal field theory (NCFT) and its gravitational dual. We suggest that a network node connecting p edges is dual to a Net-brane linking p branches in the bulk spacetime. We establish junction conditions for the Net-brane, demonstrating that they lead to energy and current conservation on the network node, which strongly supports our proposal of AdS/NCFT. We examine the typical geometries of the holographic network, notably finding that Poincaré AdS and AdS black holes serve as gravitational duals for various networks. It allows us to extend many results from AdS/CFT to AdS/NCFT. We remark that Poincaré AdS does not represent the vacuum state of a network with

⁶We assume L_{AB} is still a monotonically increasing function of l_{AB} even in the spacetime with back-reactions due to massive particles. Otherwise, the two-point correlator (5.3) could increase with l_{AB} , which is unphysical.

internal edges due to a non-trivial Casimir effect. We find that the spectrum of gravitational KK modes on the Net-brane is a mixture of that of AdS/BCFT with NBC and DBC/CBC, corresponding to the isolated and transparent modes, respectively. We also investigate two-point correlation functions in NCFTs, providing examples that include free theories and AdS/NCFT with a tensionless Net-brane.

We propose that the RT surface connects to the same intersection on the Net-brane for a connected subsystem within the network, and we validate this with the strong additivity and monotonicity of entanglement entropy. Additionally, we derive connecting conditions for the RT surfaces on the Net-brane, showing they align with the orthogonality condition for the RT surface and EOW brane in AdS/BCFT under the Z_p symmetry. We present various definitions of network entropy, with one based on the difference in entanglement entropy between NCFT and BCFT, which is always non-negative and effectively captures the network’s complexity. Finally, we briefly discuss the holographic perspective of the shortest path problem. We find it is closely related to the shortest geodesic in bulk and the holographic two-point correlators of massive operators.

Many interesting problems are worthy of exploration.

- This paper primarily focuses on simple networks. Exploring complex networks is highly intriguing, as quantum entanglement and correlation are anticipated to reveal more intricate structures and novel properties. Deep learning serves as a powerful tool for analyzing physics in complex networks. See [24–26] for the applications of deep/machine learning in holography.
- Characterizing the complexity of networks is a significant question. Deep learning suggests that artificial intelligence can only emerge when networks reach a certain level of complexity (the network is “deep” enough)⁷. The key question is: What is the threshold for this complexity? Additionally, how does this critical complexity manifest from a holographic perspective? These are essential questions of broad interest.
- This paper only discusses the HEE of a network. Studying the entanglement entropy of free theories on the network is interesting. We argue that the network entropy S_{III} is non-negative and verify it with AdS/NCFT. It is interesting to further test $S_{\text{III}} \geq 0$ with free theories.
- As mentioned earlier, Poincaré AdS is not dual to the vacuum state of a general network. It is crucial to find the gravitational dual of the vacuum state and examine the holographic bound of the Casimir effect [29, 30] for various networks.
- For simplicity, we assume the same CFTs on different edges, corresponding to the same gravity theory in different bulk branches. Studying the AdS/NCFT with different gravity parameters or theories in various branches is interesting.

⁷By “complexity”, we mean the network’s structural complexity. Please do not confuse it with the holographic complexity related to the evolution of eternal black holes [27, 28].

- Last but not least, our framework can be used to study holographic circuits and predict various electrical issues. We can construct holographic circuits by gluing geometries, such as AdS black holes with various bulk fields corresponding to resistors, capacitors, inductors, diodes, etc. Does holography establish a limit on chip computing speed or the transport coefficient between different branches? These questions are worth exploring.

Acknowledgments

Miao thanks S. He for the valuable discussions during the 30th anniversary of AEI. Miao acknowledges the supports from National Natural Science Foundation of China (NSFC) grant (No.12275366).

Note added. After we have finished the work, a paper appears in arXiv [31] with some overlaps with our paper. They focus on the holographic energy transport for 2d CFTs on intersecting lines. In comparison, we explore the gravity dual of CFTs in general networks in general dimensions.

A Killing vectors at linear order

There are no exact Killing vectors present in an arbitrary spacetime. Even locally, we can at most get a Killing vector at the linear order of coordinates. Take the network node N as an example. Near a local point on N , we can expand the metric in Riemann normal coordinates

$$ds_N^2 = \sigma_{ab} dy^a dy^b = \left(\eta_{ab} - \frac{1}{3} R_{Nacbd} y^c y^d + O(y^3) \right) dy^a dy^b, \quad (\text{A.1})$$

where R_{Nacbd} are curvatures at the origin $y^a = 0$. Solving the Killing equations $\bar{D}_{(a} \bar{\xi}_{b)} = 0$, we get $(d-1)$ local Killing vectors at the first order

$$\bar{\xi}^a = \delta^a_b + O(y^2), \quad (\text{A.2})$$

where $b = 1, 2, \dots, d-1$. In general, no Killing vectors exist at the next order $O(y^2)$, unless we impose constraints on the curvatures R_{Nacbd} .

Let us go on to discuss a local region $dV = dl dS$ including a small piece dS of the node N in the Net-brane NB or the network edges E_m . We adopt the Gauss normal coordinates $y^i = (l, y^a)$

$$\begin{aligned} ds^2 &= h_{ij} dy^i dy^j = dl^2 + \left(\sigma_{ab} - 2lk_{ab}(y) + O(l^2) \right) dy^a dy^b \\ &= dl^2 + \left(\eta_{ab} - 2lk_{ab}(0) + O(l^2, y^2, ly) \right) dy^a dy^b, \end{aligned} \quad (\text{A.3})$$

where k_{ab} are extrinsic curvatures on the node. We focus on flat network edges E_m with flat boundaries so that $k_{ab} = 0$ for edges E_m . On the other hand, the Net-brane is an asymptotically AdS spacetime and $k_{ab} \neq 0$ on its boundary generally. Solving the Killing

equations $D_{(i}\xi_{j)} = 0$ perturbatively, we obtain $(d - 1)$ local Killing vectors $\xi^i = (\xi^l, \xi^a)$ with

$$\xi^l = O(y^i)^2, \quad \xi^a = \delta^a_b - 2lk^a_b(0) + O(y^i)^2, \quad (\text{A.4})$$

where $b = 1, 2, \dots, d - 1$. The above Killing vectors obey $D_{(i}\xi_{j)} = O(y^i)$ and $n_i \xi^i = O(y^i)^2$, where $n_i = (-1, 0, \dots, 0)$ is the normal vector on the node $l = 0$.

References

- [1] J. J. Hopfield, Proc. Nat. Acad. Sci. **79**, 2554-2558 (1982)
- [2] D. E. Rumelhart, G. E. Hinton and R. J. Williams, Nature **323**, no.6088, 533-536 (1986)
- [3] G. E. Hinton and R. R. Salakhutdinov, Science **313**, no.5786, 1127647 (2006)
- [4] B. Swingle, Phys. Rev. D **86**, 065007 (2012)
- [5] P. Hayden, S. Nezami, X. L. Qi, N. Thomas, M. Walter and Z. Yang, JHEP **11**, 009 (2016)
- [6] L. Chen, X. Liu and L. Y. Hung, Phys. Rev. Lett. **127**, no.22, 221602 (2021)
- [7] G. 't Hooft, Conf. Proc. C **930308**, 284-296 (1993)
- [8] L. Susskind, J. Math. Phys. **36**, 6377-6396 (1995)
- [9] J. M. Maldacena, Int. J. Theor. Phys. **38**, 1113 (1999) [Adv. Theor. Math. Phys. **2**, 231 (1998)]
- [10] S. Ryu and T. Takayanagi, Phys. Rev. Lett. **96**, 181602 (2006)
- [11] P. Kovtun, D. T. Son and A. O. Starinets, Phys. Rev. Lett. **94**, 111601 (2005)
- [12] T. Takayanagi, Phys. Rev. Lett. **107**, 101602 (2011)
- [13] J. Y. Shen, C. Peng and L. X. Li, Phys. Rev. Lett. **133**, no.13, 131601 (2024)
- [14] R. X. Miao, JHEP **02**, 025 (2019)
- [15] C. S. Chu and R. X. Miao, JHEP **01**, 084 (2022)
- [16] G. Hayward, Phys. Rev. D **47**, 3275-3280 (1993)
- [17] H. Z. Chen, R. C. Myers, D. Neuenfeld, I. A. Reyes and J. Sandor, JHEP **10**, 166 (2020)
- [18] M. Fujita, T. Takayanagi and E. Tonni, JHEP **11**, 043 (2011)
- [19] T. M. Zhao and R. X. Miao, [arXiv:2506.20405 [quant-ph]].
- [20] D. M. McAvity and H. Osborn, Nucl. Phys. B **406**, 655-680 (1993)
- [21] C. P. Herzog and K. W. Huang, JHEP **10**, 189 (2017)
- [22] H. Liu and A. A. Tseytlin, Nucl. Phys. B **533**, 88-108 (1998)
- [23] R. X. Miao, JHEP **07**, 098 (2019)
- [24] B. Ahn, H. S. Jeong, K. Y. Kim and K. Yun, JHEP **03**, 141 (2024)
- [25] X. Chen and M. Huang, Phys. Rev. D **109**, no.5, L051902 (2024)
- [26] R. G. Cai, S. He, L. Li and H. A. Zeng, [arXiv:2406.12772 [hep-th]].
- [27] A. R. Brown, D. A. Roberts, L. Susskind, B. Swingle and Y. Zhao, Phys. Rev. Lett. **116**, no.19, 191301 (2016)

- [28] A. Belin, R. C. Myers, S. M. Ruan, G. Sárosi and A. J. Speranza, *Phys. Rev. Lett.* **128**, no.8, 081602 (2022)
- [29] R. X. Miao, [arXiv:2412.04122 [hep-th]].
- [30] R. X. Miao, *JHEP* **04**, 023 (2025)
- [31] Y. Liu and C. Y. Wang, [arXiv:2506.19553 [hep-th]].